Intraoperative Doppler and Real Time Ultrasound in Brain Surgery: Review Article

Mansour Makia, Hosni Salama, Marwan Nasr, Mohamed Mamdouh, Mohammed Elbanna
Department of Neurosurgery, Faculty of Medicine, Zagazig University
Correspondence and requests for reprints to: Marwan Nasr Ahmed Nasr
E-mail: Marwan.nasr9555@gmail.com

Article History: Received: 21.06.2023 **Revised:**04.07.2023 **Accepted:** 14.07.2023

Abstract:
Early investigation and excision are required for brain surgical lesions. When a patient has brain lesion, surgery ought to be their primary option. Treatment and total resection of a brain lesion are nearly always achievable. Maximal safe excision of brain lesions requires accurate and dependable intraoperative neuronavigation. The next frontier in navigation improvement has drawn a lot of interest in intraoperative magnetic resonance imaging, or intraoperative Magnetic Resonance Imaging (iMRI). Unfortunately, most centers throughout the world are unable to use iMRI due to its prohibitive cost and practical difficulties. By contrast, intraoperative ultrasonography (ioUS) is a low-cost instrument that can be seamlessly integrated into the theater's current setup and operational procedures. In the past, ultrasonography has been thought to have poor, artifact-prone image quality and be challenging to learn and standardize. However, with significant advancements in image quality and well-integrated navigation features over the past ten years, ioUS has undergone a dramatic evolution.

Keywords: Doppler, Ultrasound, brain surgery.

DOI: 10.53555/ecb/2023.12.1162

Introduction:

Maximal safe surgical resection is the core tenet of brain lesions intending to improve symptoms, quality of life, progression-free survival, and overall survival. However, accurate tumor localization and differentiation from surrounding functional neuronal tissue remain an ongoing challenge[(1)].

Preoperative stereotactic imaging (MRI/CT) is routinely used to plan surgical approaches. Although powerful tools, such systems are inherently limited as they do not offer real-time intraoperative representations of the tumor and surrounding structures. As surgery progresses, their accuracy deteriorates due to unpredictable brain shifts, distortions, and deformations[(1)].

Guided by non-contemporaneous inaccurate navigation, there is a risk of inadvertent damage, leading to functional deficit, or leaving residuum based on misperceived the margins, both impacting on prognosis. Consequently, there is a clear need for contemporaneous intraoperative imaging, which accurately maps the current surgical field[(2)].

Ultrasound (US) is an affordable, safe, repeatable imaging technique that can be easily integrated into surgical workflow allowing live imaging during surgery. Over the last 30 years, US has matured as a neurosurgical tool, becoming established in routine practice in many neurosurgical centers[3].

Ultrasound (US) was first applied to adult neurosurgery in 1982, at which time the advent of 2-dimensional B-mode imaging (2D US) allowed real-time visualization of neural anatomy and pathology during surgical interventions. Since then, intraoperative ultrasound has allowed surgeons to craft and update operative plans with without ionizing radiation exposure or major workflow interruption[4].

Doppler ultrasonography can be used to assess lesion vascularity and to plan the operative approach. Doppler ultrasonography utilizes the Doppler's effect, which is an observed frequency shift when a US wave is reflected back to the transducer from moving particles, to determine the direction and relative velocity of fluid along the axis of the probe[5].

There are subtypes of Doppler imaging that are based on this general principle. Color Doppler imaging relies on the magnitude of measured Doppler shift and, in a selected portion of the US frame, shows with color the direction of flow, either toward or away from the probe, overlaid on the 2D US image[6].

Color Doppler is very angle dependent: at any point where flow is perpendicular to the US waves, no Doppler shift and therefore, no flow, will be observed. Therefore, a change in angle and a change in velocity may appear similarly on color Doppler [7].

Furthermore, color Doppler suffers from aliasing, an artifact in which areas of flow are represented with incorrect magnitude or direction as a result of transducer pulse rate limitations. Finally, color Doppler imaging is highly susceptible to noise, which may overwhelm the flow signal[8].

Power Doppler, which relies on the power of the Doppler shift signal instead of the magnitude of the shift, was developed as an alternative to color Doppler imaging. As compared to color Doppler, power Doppler has less noise, less angle dependence, greater resolution of small vessels, and no aliasing[9].

Power Doppler, however, sacrifices information about flow direction and velocity. The power Doppler signal also tends to be visible outside the boundaries of blood vessels and, as such, vessels appear larger on power Doppler imaging than they do on MRA[10] .

In addition, the high sensitivity of power Doppler may result in visualization of small vessels of limited relevance, thus diminishing intraoperative utility. Finally, power Doppler is limited by operator dependence, motion sensitivity artifacts, and overall poor resolution compared to other imaging modalities[11].

Anatomy of Brain:

While the brain is 2% of the total body mass, it uses nearly 50% of the human body's glucose. This makes it the most energy-intensive organ of the human body. Thus, the brain ought also to be one of the most perfused organs in the body[12].

Two major sources of arterial blood provide this perfusion: the anterior circulation that originates in the internal carotid arteries and the posterior (or vertebrobasilar) circulation that originates in the vertebral arteries[13].

The cerebral circulation originates in the left heart and is conducted by the arch of aorta, which gives rise to three branches. The first and largest branch is the brachiocephalic trunk; the second branch is the left common carotid artery; and the third is the left subclavian artery, which ascends with the left common carotid artery through the superior mediastinum and along the left side of the trachea[14].

The vertebral arteries arise as the most proximal ascending branch from the subclavian arteries on each side of the body and enter deep into the cervical vertebral transverse processes, typically at the level of the 6th cervical vertebra[15].

The arteries proceed superiorly in the transverse foramen of each cervical vertebra, passing through the transverse foramen of the atlas (C1). Once here, they make a sharp posterior bend, traveling across the posterior arch of C1 and through the suboccipital triangle, piercing the dura mater on their way toward the foramen magnum. Passage through the foramen magnum marks the beginning of the arteries' intracranial course[16].

The left common carotid artery arises directly from the aortic arch, the right internal carotid artery (ICA) arises from the brachiocephalic trunk which originates on the right side of the chest near the trachea, and bifurcates posterior to the sternoclavicular joint into the right subclavian artery and right common carotid artery as it moves rightward within the superior mediastinum[17].

On the left side of the body, however, there is no brachiocephalic trunk: on this side, the common carotid artery comes directly from the aortic arch as its second branch[18].

Following their entry into the cranial cavity, the internal carotid and vertebral arteries fulfill the formidable role of exclusive suppliers of the blood necessary to maintain the brain in addition to drain interstitial fluid and protein from the brain[19].

Both circulatory divisions provide major branches to the diencephalic and telencephalic regions of the brain proper. To do so, the circulations first meet as the Circle of Willis[20].

The branches of the circle are as follows: the anterior cerebral artery (ACA), anterior communicating artery (ACoA), internal carotid artery (ICA), posterior cerebral artery (PCA), posterior communicating artery (PCoA), and basilar artery[21]. **[Figure 1]**

From their origin within the interpeduncular fossa, these branches course centrifugally toward their divergent cerebral targets, becoming the cerebral arteries that are grossly visible covering the cortical surface[22] .

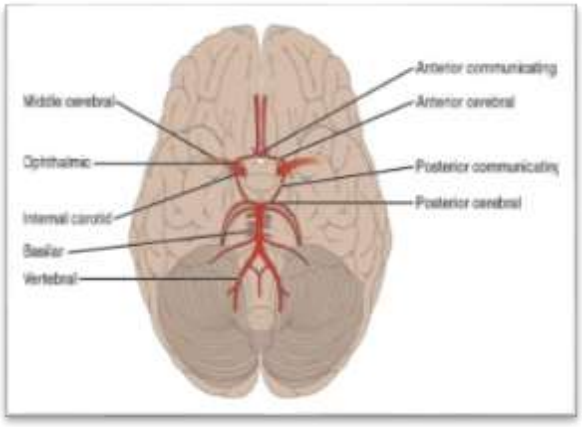

Figure (1): Schematic of the circle of Willis and cerebral vasculature in relation to local anatomy

The Anterior Cerebral Circulation:

The anterior cerebral circulation is composed of branches from the ICA. The anterior cerebral artery, middle cerebral artery, and the anterior choroidal artery are highly prominent and pathophysiologically significant[23].

The function of the anterior division of the cerebral circulation is to supply blood to a large proportion of the forebrain, including the frontal, temporal, and parietal lobes, as well as parts of the diencephalon and internal capsule[17].

Anterior cerebral artery:

The anterior cerebral artery primarily supplies blood to the most medial aspect of the cerebral cortical surface, located along the longitudinal fissure. This area includes portions of the frontal lobes, as well as the superomedial parietal lobes[24].

Its course is as follows: after arising from the anterior clinoid portion of the ICA, it courses anteromedially over the superior surface of the optic chiasm, toward the longitudinal fissure. Shortly after arrival in the fissure, it forms an anastomosis with the contralateral ACA. This anastomosis is called the anterior communicating artery. It also marks the first segmental division of the ACA, which is divided regionally into five segments along its course: A1–A5[25] **[Figure 2].**

As the ACA proceeds, then, beyond A1, it begins its posterior course toward the parieto-occipital sulcus, following the contour of the callosal sulcus between the two cerebral hemispheres. The ACA provides deep and cortical branches; these arise from the proximal and distal portions of ACA, respectively[26].

Table (1): Anterior cerebral artery segments and their blood supply

Segment	Boundaries	Branches	Regions supplied	Important variants
A1	Between ICA and ACoA	Medial lenticulostriate artery; ACoA; small arterial branches to perforated substance, subfrontal area, dorsal surface of optic chiasm, hypothalamus, and suprachiasmatic nucleus	Caudate nucleus and anterior limb of the internal capsule, anterior hypothalamus, septum pellucidum, anterior commissure, fornix, and the anterior striatum	Fenestrated A1: Rare, it is associated with aneurysms
A2	ACoA to the bifurcation forming the pericallosal and supramarginal arteries	Recurrent artery of Heubner (may also arrive from A1, rarely), orbitofrontal artery and frontopolar artery, small arterial branches to perforated substance, subfrontal area, dorsal surface of optic chiasm, hypothalamus, and	Anterior portion of caudate nucleus, Internal capsule, inferior and inferomedial surfaces of the frontal lobe including gyri recti	Superior anterior CoA: An anomalous communicating vessel between the ACAs near the corpus callosum has been associated with aneurysms

		suprachiasmatic nucleus		
A3	Pericallosal sulcus, extends around genu of corpus callosum	Superior and inferior internal parietal arteries, precuneal artery, callosal marginal artery (present only in 60% of cases)	Corpus callosum, superior frontal gyrus, precuneus, and medial aspect of hemisphere above corpus callosum	Contralateral hemisphere supply: In about 64% of people, A3 has branches supplying the contralateral hemisphere
A4 and A5	Smaller branches that go over corpus callosum	Callosal arteries (smaller arteries)	Corpus callosum	

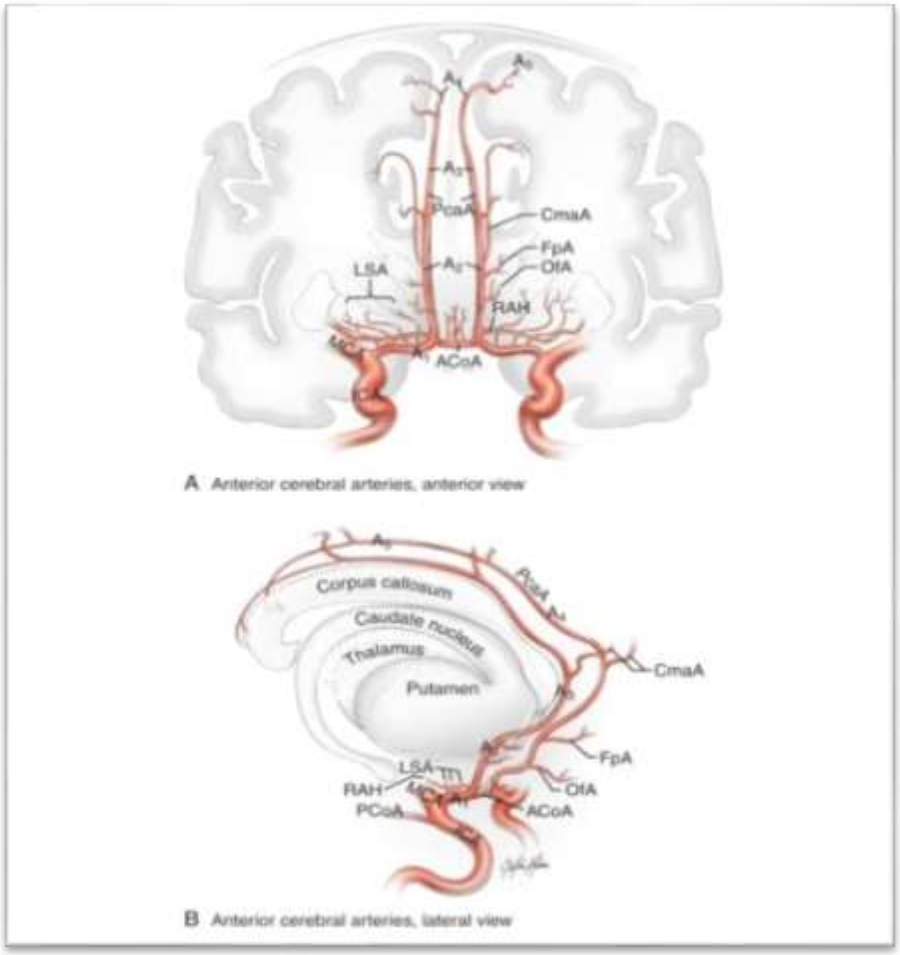

Figure (2): Anterior cerebral segments

Anterior choroidal artery:

Anterior choroidal artery is a branch of the ICA that typically arises from the supraclinoid portion, just before the bifurcation of the middle and anterior cerebral arteries. Although rare, still other variations have also been observed, including complete absence, as well as duplication, of AChA[27].

The AChA gives off both deep and superficial branches. The deep branches includes the posterior two-thirds of the

internal capsule, adjacent optic and auditory radiations, medial portion of the globus pallidus, and tail of the caudate nucleus; the superficial branches includes piriform cortex and uncus, hippocampal head, amygdala, and most lateral portion of the thalamic lateral geniculate nucleus[28].

Middle cerebral artery:

Middle cerebral artery is the largest and most complexly distributed of the cerebral vessels, supplying many critical cerebral structures along its sinuous course. The artery has a relatively consistent route: variations have been found in 3.8% of patients, and have not been determined to be of clinical significance[29].

It originates from the bifurcation of the ICA, just lateral to the optic chiasm at the medial end of the Sylvian fissure, and passes laterally from there along the ventral surface of the frontal lobe, entering the Sylvian fissure between the temporal lobe and insular cortex[30]. **[Figure 3]**

Within this region, the artery typically bifurcates or trifurcates, giving rise to two or three principal trunks. These, in turn, extend superiorly and inferiorly over the insular surface, supplying, by means of an arterial arborization that ultimately extends over most of the lateral surface of the cerebral hemisphere.

The following cortical territories: all of the insular cortex and opercular surface, the superior and middle temporal gyri, a parietal territory that comprehends the inferior parietal lobule and much of the postcentral gyrus, and a frontal territory that comprehends inferior and middle frontal gyri, much of the precentral gyrus, and the lateral part of the orbital surface. **[Table 2]**

Table (2): Middle cerebral artery segments and their supply

Segment	Anatomic path	Branches	Areas supplied
M1 (horizontal)	Originates at carotid bifurcation, becomes middle cerebral artery, and branches turn superiorly into the area between temporal lobe and insula	Medial and lateral lenticulostriate arteries (15-17 in number) and anterior temporal artery	Head and body of the caudate nucleus, the upper part of the anterior limb, the genu and anterior portion of the posterior limb of internal capsule, the putamen and the lateral pallidum and anterior temporal lobe
65M2 (insular)	Entry point at temporal lobe and insula, ascends along the insular cleft and makes a hairpin turn at the insular sulcus	Terminal branches: 2-3 main trunks Superior division: Orbitofrontal artery, prefrontal artery, precentral artery, and central arteries Inferior division: Temporopolar artery, temporo-occipital artery, angular artery and anterior, middle and posterior temporal arteries	Superior division: Orbitofrontal area to the posterior parietal love Inferior division: Temporal pole to the angular area of parietal lobe
M3 (opercular)	Begins at the apex of the hairpin turn in the insular sulcus and terminates as the branches reach the lateral convexity of the cerebral hemisphere	Terminal branches/2-3 main trunks: Upper and lower trunks	Frontal, parietal, and temporal operculae
M4 (cortical)	Begins at the surface of the	Cortical branches	Hemispheric surface of

	Sylvian fissure, extends over cerebral hemisphere and arises between frontal, parietal and temporal lobes		frontal and parietal lobes

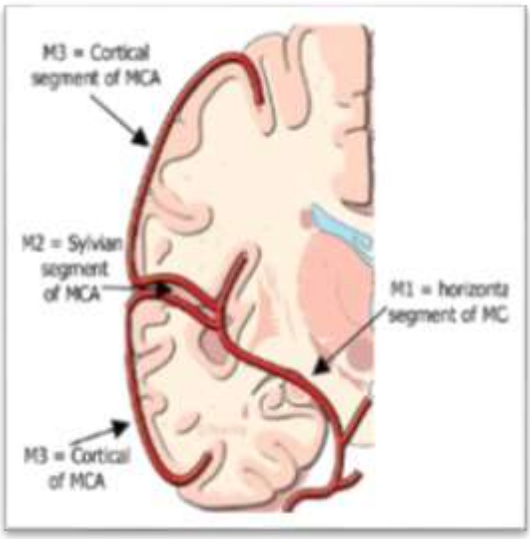

Figure (3): M1, M2 and M3 segments of the middle cerebral artery

The Posterior Cerebral Circulation:

The posterior cerebral circulation maintains many of the nervous system's most critical functions. Also known as the vertebrobasilar circulation, it is comprised of the vertebral arteries, the basilar artery into which the vertebrals fuse, and several branches from these main conduits[(31)].

This circulation supplies blood to the posterior portion of the brain that includes the occipital lobe, most of the anterior and posterior portions of the brainstem, and all of the cerebellum[(32)]**.**

Vertebral arteries:

These are paired, bilaterally symmetrical arteries that arise from the subclavian vessels on each side of the body. Like the MCA, they have been partitioned into four segments. Unlike MCA, the first three of these segments are extracranial[(33)]**.**

The most proximal segment, V1, extends from the vessels' subclavian origin to the vertebral transverse foramen. The succeeding V2 segment then courses through the transverse foramen. V3 loops from approximately the level of C2 around the atlas and then enters the dura[(34)]. **[Figure 4]** Once through the dura, the arteries become V4 which is the intracranial segment of the vertebral arteries. Immediately after entering the brain through the foramen magnum, it gives rise to two important branches. The first is the posterior inferior cerebellar artery (PICA), and the Second is anterior spinal artery[(35)].

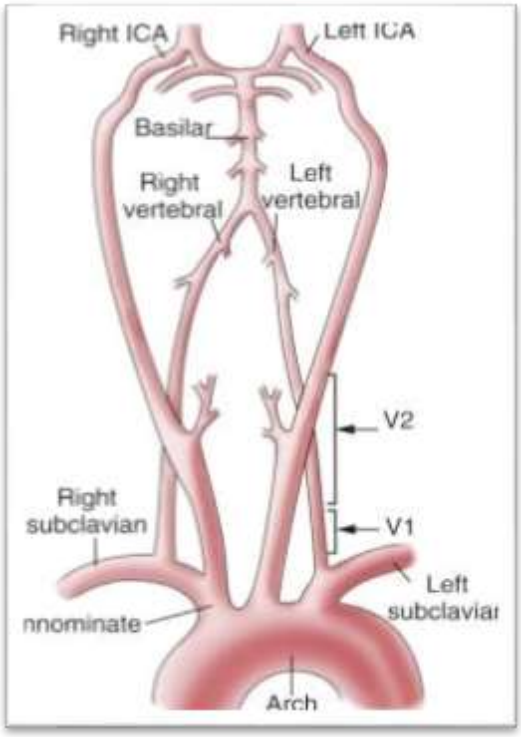

Figure (4): Anatomy and segments of the vertebral artery**.**

Posterior inferior cerebellar artery:

Posterior inferior cerebellar artery is the largest branch of the vertebral artery. After splitting off from its vertebral origin, it winds posteriorly around the upper medulla,

passes between the origins of the vagus and accessory nerves, and then proceeds along the inferior cerebellar peduncle to reach the ventral surface of the cerebellum, where it divides into medial and lateral branches[36].

The artery provides blood to the part of the medulla and cerebellum corresponding to its course: the dorsolateral region of the medulla and a region of the ventral surface of the cerebellar hemispheres that includes the inferior vermis[37].

Basilar artery:

The paired V4 segments give way to a single basilar artery after its anastomosis at the pontomedullary junction that travels along the midline anterior pons, and terminates near the pontomesencephalic junction[38]. **[Figure 5] .**

During its course, the artery branches providing several perforating arteries to the pons, the anterior inferior cerebellar and superior cerebellar arteries to a broad cerebellar territory, and then supplies much of the posterior cortical surface through its terminal split into the posterior cerebral arteries[39].

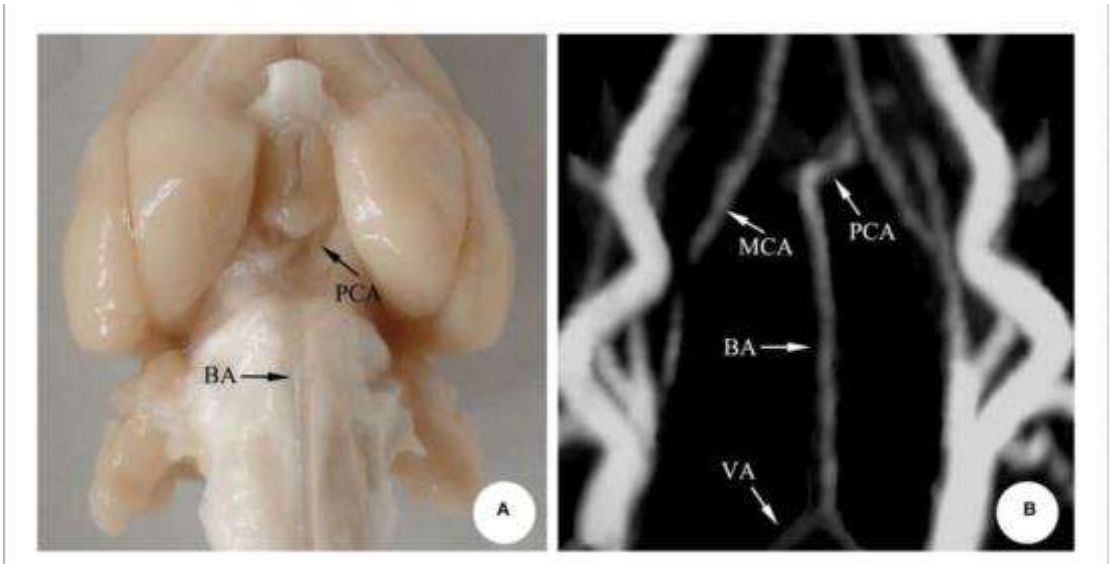

Figure (5): The basilar artery (A) Microscopic anatomy; (B) D-TOF-MRA. BA, Basilar artery; PCA, Posterior cerebral artery; VA, Vertebral artery; MCA, Middle cerebral artery **.**

Pontine branches:

These arteries are small, numerous, basilar branches that supply the pontine brainstem. When categorized according to distribution, they fall into two classes[40].

The first class, referred to as paramedian, extends immediately from the basilar artery into the substance of the pons and supplies the corticospinal tract. The second class is called circumflex which extends its longest branches all the way around to the dorsal aspect of the pons as posterior pontine arteries[41].

Anterior inferior cerebellar artery:

Anterior inferior cerebellar artery is the first large branch of the basilar artery. It generally proceeds from the caudal one-third of the basilar artery, traveling laterally along the middle cerebellar peduncle to reach the cerebellum In addition to supplying the petrosal surface of the cerebellum[42].

It also supplies a subregion of the pontine brainstem that includes the middle cerebellar peduncle, and the central portions of several sensory pathways. In addition, it

gives rise to the labyrinthine artery of the inner ear[43].

Superior cerebellar artery:

Superior cerebellar artery is the final, nonterminal branch of the basilar artery. It runs laterally over the superior cerebellar peduncle, supplying the peduncle itself and much of the superior surface of the cerebellum. It also supplies the deep nuclei embedded within the cerebellar white matter, and a brainstem region adjacent to the rostral pontine tegmentum[37].

Posterior cerebral artery:

The final posterior circulation contribution to consider is that provided by the posterior cerebral arteries. These arteries usually arise bilaterally from the terminal bifurcation of the basilar arteries but have been found to originate unilaterally at the ICA in between 11% and 29% of cases examined[44].

After splitting from the basilar artery, the PCA encircles the midbrain at the pontomesencephalic junction. Along its posterior passage, it travels over the cerebral peduncles, and thence to the ventromedial surface of the cortex supplying the occipital lobe, the inferior and medial parts of the temporal lobe, and a posterior portion of the inferior parietal lobe[45] **[Figure 6].**

PCA also has a substantial subcortical territory that covers the thalamus, midbrain, and choroid plexus. Like the ACA and MCA of the anterior circulation, the PCA has been divided into segments by location along its extent[46].

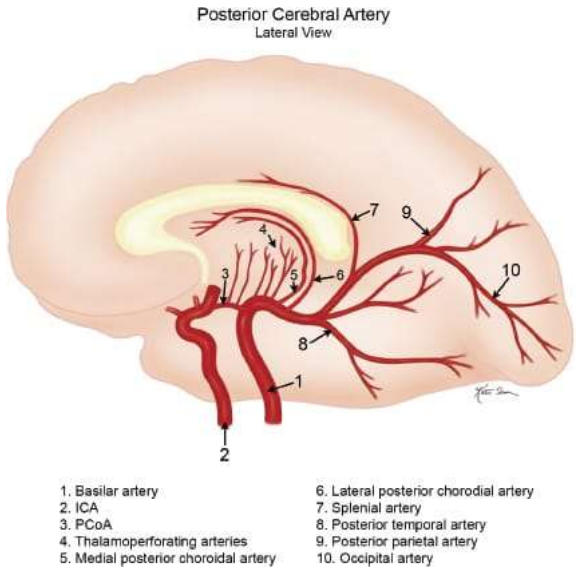

Figure (6): Lateral view of the posterior cerebral artery and its branches.

The Cerebral Venous System:

The cerebral venous system can be divided into two anastomosing networks according to position with respect to the cortical surface: the more superficially located dural venous sinuses, and the deeper cerebral veins[47] .

Dural venous sinuses are endothelially lined channels. Their general function is collection of venous blood from the cerebral veins, and the delivery of this blood to the systemic venous circulation. They are usually formed between the outer (periosteal) and inner (meningeal) layers of dura mater, located adjacent to the osseous surfaces inside the cranium[48] .

The confluence of sinuses (CS) or the torcular Herophili is one of the major sinuses, and a pooling point for venous blood destined. It is located at the occipital pole of the cranial cavity and is formed by the junction of several of the other sinuses.

These include the superior sagittal sinus that runs along the calvaria through the

falx cerebri; the straight sinus that represents the continuation of the inferior sagittal sinus and great cerebral vein of Galen; the occipital sinus just inferior to the CS; and the transverse sinuses that traverse the base of the occipital bone[49]. **[Figure 7]**

The inferior sagittal sinus runs in the inferior concave free border of the cerebral falx. As mentioned, this sinus continues as the straight sinus, running between the falx cerebri and tentorium cerebelli to join the CS[50] **.**

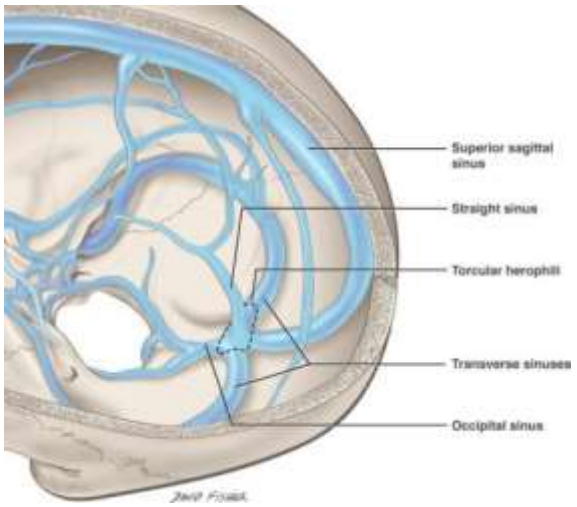

Figure (7): The Torcular Herophili[51]

The bilateral cavernous sinuses are located superior to the body of the sphenoid bone and demarcated by the superior orbital fissure anteriorly, the temporal bone posterity, and the sella turcica medially, these sinuses receive blood from the superior and inferior ophthalmic veins, superficial middle cerebral veins, sphenoparietal sinuses, and inferior cerebral veins[52] **.**

Two intercavernous sinuses (an anterior and a posterior) connect the two cavernous sinuses across the midline. Two sets of petrosal sinuses then drain the cavernous sinuses: the superior petrosal and the inferior petrosal sinuses[53]. **[Figure 8] .**

The inferior petrosal sinuses are interconnected by the basilar venous plexus. The sigmoid sinus is a continuation of the transverse sinuses that passes inferiorly in an "S"-shaped groove posteromedial to the jugular foramen, and serves to channel cerebral venous blood to the internal jugular vein[54].

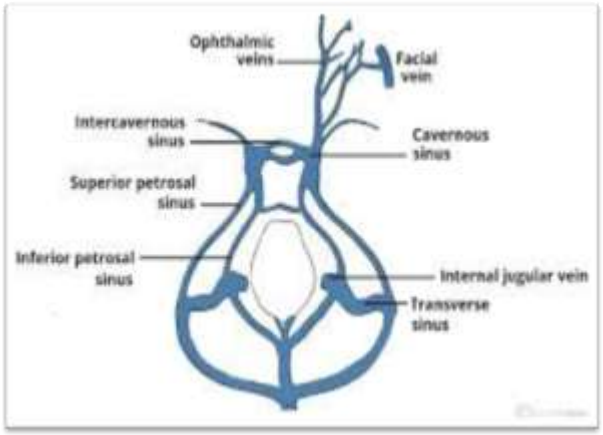

Figure (8): Schematic of the dural venous system relating to the cavernous sinus[55]

The deep cerebral veins are distinguished from the superficial veins both by position and by drainage polarity: while the superficial veins drain centrifugally toward the lateral parts of the sinus system, the deep veins drain centripetally, converging at midline as the great cerebral veinof Galen[56] **.**

Ultrasound physics:

Diagnostic ultrasound employs a piezoelectric transducer to convert electrical signals into sound waves at above audible frequencies (between 1-20 MHz). These acoustic pressure waves are transmitted into tissue and either absorbed, scattered, or reflected, based on the wavelength and frequency of the wave and the inherent physical acoustic qualities of the tissue. The sound waves reflected as echoes are detected

by the same piezoelectric transducer and converted to an electrical signal **(57).**

Ultrasound propagation depends on the tissues acoustic impedance (Z), which is determined by the product of the tissues density (ρ) and the velocity of sound (c), which relates to the elasticity of the tissue ($Z = \rho c$). Reflection of sound waves occurs at tissue interfaces where there is a change in acoustic impedance. The echogenicity of structures on US relates to the amplitude of the reflected signal, which is proportional with an interfaces acoustic gradient**(58).**

For instance, choroid plexus has a high acoustic gradient with the adjacent brain and is hyperechoic, while the low density, low acoustic impedance, homogenous CSF-filled ventricles are hypoechoic. The majority of echoes in the body arise from smaller interfaces known as diffuse reflectors, which account for the characteristic speckled echotexture seen on US in different tissues**(1).**

In addition to reflection, acoustic energy is also attenuated predominantly by absorption as heat and refraction. The higher the US frequency, the better the resolution is. But, the greater the degree of attenuation, Resultantly high-frequency probes are best for detailed imaging of superficial structures, and low-frequency, lower resolution probes are superior for visualizing deeper structures and providing a greater field of view**(59) .**

Optimizing image quality:

In any image-guided procedure, optimal image quality is essential for optimal accuracy. Poor image quality was associated with significantly worse postoperative functional outcome. Image quality in Doppler US is highly variable and operator-dependent. Unlike CT/MRI, which can image the entire head in three dimensions, intraoperative Doppler ultrasound is restricted to the craniotomy from which there is a limited field of view**(60).**

US has the potential for infinite different brain views, which are dependent on craniotomy location, probe type and probe orientation. To the uninitiated, the unfamiliar perspective and tomographic representation can be bewildering. The many different probes, settings, and potential artifacts steepen this learning curve**(1)**.

With careful preparation and a consistent approach, good image quality can be achieved. To encourage a systematic approach and facilitate comparison between US and MRI, performing US sweeps in two orthogonal planes approximated to conventional anatomical planes is useful**(61)**.

Standardization is also needed to allow comparability and generalization between different operators and units. Extending from this, assessment the role of US in glioblastoma resection in the UK-based randomized controlled trial titled Functional and Ultrasound-Guided Resection of glioblastoma (FUTURE-GB) was performed. This trial evaluates the impact of US and diffusion tensor imaging-guided resection on deterioration-free survival **[Figure 10]**

Probe choice:

There are various probes, each with different strengths and limitations. Generally, small footprint probes are favored for intraoperative use as the craniotomy can accommodate them. There are three main types of transducer: linear,

curved, and sector array. Historically, linear and curved transducers had large footprints and were limited to large craniotomies[(62)].

One of the most widely used probes is a type of sector array transducer known as a phased array, a low-frequency, small foot-print probe, through which a large trapezoid field of view of the brain can be produced through a small craniotomy window. Unfortunately, phased array probes are low resolution and are particularly vulnerable to image deterioration. Recently, smaller footprint linear and curved array probes have become available, which offer better resolution[(1)] **[Table 3].**

In a series comparing iMRI to a conventional phased array probe and a small footprint linear probe, sensitivity for tumor residual by linear ultrasound (79%) was almost equivalent to iMRI (83%) and far superior to the conventional phased array probe (21%). Linear probes also demonstrate significantly better residual detection and better visualization of vascularity than the phased array probe, with an improved extent of resection (EOR) in 75% of cases[(63)] **.**

Artifacts:

Imaging artifacts could result in missed residual disease or, conversely damaging, over-aggressive resection of normal brain that has been misrecognized as tumor. The most frequently encountered artifacts are acoustic shadowing (AS) and posterior wall acoustic enhancement (PAE)

Acoustic shadowing occurs deep to interfaces where there is complete reflection or absorption of US, typically when there is a marked acoustic gradient or where structures strongly absorb acoustic energy, for instance, at the brain-skull interface. Gas bubbles in the surgical site or trapped within the sheathed ultrasound probe are a common source of AS[(64)] **[Figure 10]**

Gas bubbles can also cause ring-down artifact, which occurs when an ultrasound pulse encounters small fluid collections trapped between several gas bubbles. This trapped fluid resonates, producing a continuous signal back to the transducer, which generates an echogenic "step-ladder" like artifact shadow. Hemostatic material is particularly recognized as a cause of ring-down artifact as it can retain multiple gas locules[(1)]**.**

Posterior wall acoustic enhancement appears beneath fluid containing homogenous structures, such as cysts and fluid-filled resection cavities. Fluid attenuates US less than solid tissue, consequently deep to fluid, there are stronger sound beams that generate echoes of greater amplitude and thus greater echogenicity. Differentiating residual echogenic tumor from PAE can be difficult at the floor of a resection cavity[(65)]**.**

PAE occurs parallel to the US beam and is often linear in morphology; thus, moving the US probe and careful assessment of changes in its appearance can facilitate detection. Tangential placement of the probe on adjacent preserved cortex angulated toward the floor of the resection can also reduce PAE[(66)]**.**

Coagulated blood, contusion, and edema also alter the appearance of the surgical field. Blood and contusion are particularly challenging as these appear echogenic, with features similar to residual disease. Intracavitary linear transducers are better at discerning residuum from other surgery-related changes[(67)]**.**

Careful correlation with the preoperative navigation MRI and prior earlier US scans is essential, as lesion will be present on all images, while artifacts, such as PAE and surgical changes, will have developed over the surgical period[(68)].

References:

1- Dixon, L., Lim, A., Grech-Sollars, M., Nandi, D., & Camp, S. (2022). Intraoperative ultrasound in brain tumor surgery: A review and implementation guide. Neurosurgical Review, 45(4), 2503–2515.

2- Pino, M. A., Imperato, A., Musca, I., Maugeri, R., Giammalva, G. R., Costantino, G., Graziano, F., Meli, F., Francaviglia, N., Iacopino, D. G., & Villa, A. (2018). New hope in brain glioma surgery: The role of intraoperative ultrasound. a review. Brain Sciences, 8(11), 202.

3- Ganau, M., Ligarotti, G. K., & Apostolopoulos, V. (2019). Real-time intraoperative ultrasound in brain surgery: neuronavigation and use of contrast-enhanced image fusion. Quantitative Imaging in Medicine and Surgery, 9(3), 350–358.

4- Zeineldin, R. A. (2023). Deep multimodality image-guided system for assisting neurosurgery. ResearchGate.

5- Moradi, S., Ferdinando, H., Zienkiewicz, A., Sarestoniemi, M., & Myllylä, T. (2022). Measurement of cerebral circulation in human. In IntechOpen eBooks.

6- Maulik, D. (2023). Doppler color flow: basic principles. In Springer eBooks (pp. 81–98).

7- Meola, M., Ibeas, J., Lasalle, G., & Petrucci, I. (2021). Basics for performing a high-quality color Doppler sonography of the vascular access. Journal of Vascular Access, 22(1_suppl), 18–31.

8- Hacking, C., & Botz, B. (2018). Aliasing phenomenon (ultrasound). Radiopaedia.org.

9- Evans, D. H. (2021). Transcranial doppler Ultrasound: physical principles. In Springer eBooks (pp. 99–116).

10- Settecase, F., & Rayz, V. L. (2021). Advanced vascular imaging techniques. In Elsevier eBooks (pp. 81–105).

11- Kananeh, M., & Shah, S. O. (2021). Management of brain tumors in ICU: Monitoring the neurological impact by transcranial Doppler (TCD/TCCS). In Springer eBooks (pp. 931–936).

12- Tang, B., Luo, Z., Zhang, R., Zhang, D., Nie, G., Li, M., & Yan, D. (2023). An update on the molecular mechanism and pharmacological interventions for Ischemia-reperfusion injury by regulating AMPK/mTOR signaling pathway in autophagy. Cellular Signalling, 107, 110665.

13- Di Pietro, M., Di Stefano, V., Cannella, R., Di Blasio, F., & De Angelis, M. V. (2021). Fetal variant of posterior cerebral artery: just a physiologic variant or a window for possible ischemic stroke? Neurological Sciences, 42(6), 2535–2538.

14- Shang, T., Tian, L., Li, D., Wu, Z., & Zhang, H. (2018). Favourable Outcomes of Endovascular Total Aortic Arch Repair Via Needle Based In Situ Fenestration at a Mean Follow-Up of 5.4 Months. European Journal of Vascular and Endovascular Surgery, 55(3), 369–376.

15- Yi, X., Xie, P., Zhang, L., Lu, F., Chen, H., & Liu, K. (2022). Entrance and origin of the extracranial vertebral artery found on computed tomography angiography. Scientific Reports, 12.

16- Lateral neck swellings. (n.d.). Google Books.

17- Reviews in Neurology 2019. (n.d.). Google Books.

18- Europe PMC. (n.d.). Europe PMC. European Journal of Vascular and Endovascular Surgery, 55(3), 369–376.

19- Nolte's The Human Brain. (n.d.). Google Books.

20- Ishikawa, Y., Yamamoto, N., & Hagio, H. (2022). From Neural Tube to Larval Brain: Blood Vessels and Proliferative Zones. In neurosurgery (pp. 123–132).

21- Liu, Y., Zhu, L., Hou, B., Wang, T., Xu, D., Tan, C., Zhang, H., Li, C., & Wang, J. (2021). Study on the correlation between the circle of Willis structure and collateral circulation in bilateral carotid artery occlusion. Neurological Sciences, 42.

22- Drake R, Vogl AW, Mitchell AW. Gray's Anatomy for Students. 3rd ed. xxv. Philadelphia, PA: Churchill Livingstone/Elsevier; 2015. p. 1161.

23- Komatsu, T., Ohta, H., Motegi, H., Hata, J., Terawaki, K., Koizumi, M., Muta, K., Okano, H. J., & Iguchi, Y. (2021). A novel model of ischemia in rats with middle cerebral artery occlusion using a microcatheter and zirconia ball under fluoroscopy. Scientific Reports, 11.

24- Pradip, C., Rathawa, A., Jethwa, K., & Mehra, S. (2021). The anatomy of the cerebral cortex. In Exon Publications eBooks (pp. 1–16).

25- Importance of magnetic resonance imaging in acute infarct - ProQuest. (n.d.).

26- Rhoton's cranial anatomy and surgical approaches. (n.d.). Google Books.

27- Srinivasan, V. M., Ghali, M. G. Z., Cherian, J., Mokin, M., Puri, A. S., Grandhi, R., Chen, S. R., Johnson, J. N., & Kan, P. (2017). Flow diversion for anterior choroidal artery (AChA) aneurysms: a multi-institutional experience. Journal of NeuroInterventional Surgery, 10(7), 634–637.

28- Emos, M. C. (2023, June 5). Neuroanatomy, internal capsule. StatPearls - NCBI Bookshelf.

29- Navarro-Orozco, D. (2023, July 24). Neuroanatomy, middle cerebral artery. StatPearls - NCBI Bookshelf.

30- Poblete, T., Casanova, D., Soto, M. A., Campero, A., & Mura, J. (2021). Microsurgical anatomy of the anterior circulation of the brain adjusted to the neurosurgeon's daily practice. Brain Sciences, 11(4), 519.

31- Gomez, F., Amuluru, K., Elkun, Y., & Al-Mufti, F. (2021). Cryptogenic stroke and stroke of "Unknown

cause." In Springer eBooks (pp. 293–322).

32- Bazira, P. J. (2021). An overview of the nervous system. Surgery (Oxford), 39(8), 451–462.

33- Ota, T. (2022). Functional arterial anatomy of the brain. Stroke: Vascular and Interventional Neurology, 2.

34- Atlas of Intraoperative cranial Nerve Monitoring in thyroid and head and neck surgery. (n.d.). Google Books.

35- Rajasekaran, R., Ray, P., Ramesh, S. V., Devadas, A. K., Joshua, T. V., Balamurugan, A., Ramesh, M. K., & Rajasekaran, R. (2022). Cerebral arterial circulation: 3D augmented reality models and 3D printed puzzle models. In *IntechOpen eBooks*.

36- Ocak, P. E., Dogan, I., Sayyahmelli, S., & Baskaya, M. K. (2019). Retrosigmoid approach for vestibular Schwannoma surgery. In Springer eBooks (pp. 105–133).

37- Chaddad-Neto, F., & Da Costa, M. D. S. (2022). Surgical anatomy of the medulla oblongata. In Springer eBooks (pp. 199–215). **Chandra, A., Li, W. A., Stone, C., Xu, G., & Ding, Y. (2017).** The cerebral circulation and cerebrovascular disease I: Anatomy circle of Willis structure and collateral circulation in bilateral carotid artery occlusion. Neurological Sciences.

38- Catalano, M., Crimi, L., Belfiore, G., Grippaldi, D., David, E., Spatola, C., Cristaudo, C., Foti, P. V., Palmucci, S., & Basile, A. (2023). Congenital and acquired anomalies of the basilar artery: A pictorial essay. Rivista Di Neuroradiologia.

39- Nuñez, M., Guillotte, A. R., Faraji, A. H., Deng, H., & Goldschmidt, E. (2021). Blood supply to the corticospinal tract: A pictorial review with application to cranial surgery and stroke. Clinical Anatomy, 34(8), 1224–1232.

40- Vlašković, T., Brkic, B. G., Stevic, Z., Vukicevic, M., Đurović, O., Kostic, D., Stanisavljevic, N., Marinkovic, I., Kapor, S., & Marinković, S. (2022). Anatomic and MRI Bases for Pontine Infarctions with Patients Presentation. Journal of Stroke and Cerebrovascular Diseases, 31(8), 106613.

41- Vogels, V. I., Dammers, R., Van Bilsen, M., & Volovici, V. (2021). Deep cerebral perforators: anatomical distribution and clinical symptoms. Stroke, 52(10).

42- Donkelaar, H. J. T., Comert, A., Van Der Vliet, T., Van Domburg, P., & Wesseling, P. (2020). Vascularization of the brain and spinal cord. In Springer eBooks (pp. 71–126).

43- Naydin, S., Marquez, B., & Liebman, K. (2022). Vascular anatomy of the brain. In Springer eBooks (pp. 3–29). https://doi.org/10.1007/978-3-030-88196-2_1Neurology (pp. 55–71). \

44- Bonasia, S., Smajda, S., Ciccio, G., Bojanowski, M. W., & Robert, T. (2023). Proposed new classification for internal carotid artery segmental agenesis based on embryologic and angiographic correlation. Surgical and Radiologic Anatomy, 45(4), 375–387.

45- Posterior Cerebral artery stroke. (2023, January 1). PubMed.

https://pubmed.ncbi.nlm.nih.gov/30335329/

46- The human brainstem. (n.d.). Google Books.

47- Tabani, H., Meybodi, A. T., & Benet, A. (2020). Venous anatomy of the supratentorial compartment. In Handbook of Clinical Neurology (pp. 55–71).

48- Sarma, A., Martin, D., Pruthi, S., Jones, R. A., & Little, S. B. (2023). Imaging the cerebral veins in pediatric patients: Beyond dural venous sinus thrombosis. Radiographics, 43.

49- Yamane, F., Michiwaki, Y., Tanaka, T., Matsuno, A., Kohyama, S., Uno, T., Oyama, Y., & Ito, A. (2022). Structural Analysis of Tentorial Dural Arteriovenous Fistulae with Special Considerations of Venous Ectasia: Proposing a Simpler Classification. In neurosurgery (pp. 187–202).

50- Brain anatomy and neurosurgical approaches. (n.d.). Google Books. false Brain Circulation, 3(2).

51- Granger, A., & Tubbs, R. S. (2020). The torcular herophili (Confluence of sinuses). In Elsevier eBooks (pp. 71–85).

52- Massa, R. N. (2023, July 24). Neuroanatomy, cavernous sinus. StatPearls - NCBI Bookshelf.

53- Balcerzak, A., Tubbs, R. S., Zielinska, N., & Olewnik, Ł. (2023). Clinical analysis of cavernous sinus anatomy, pathologies, diagnostics, surgical management and complications – Comprehensive review. *Annals of Anatomy-anatomischer Anzeiger*, *245*, 152004.

54- Anatomy, imaging and surgery of the intracranial dural venous sinuses. (n.d.).

55- TeachMeAnatomy. (2023, July 18). The Cavernous Sinus - Contents - Borders - Thrombosis - TeachMeAnatomy.

56- Rasmussen, M. K., & Mestre, H. (2022). Fluid transport in the brain. Physiological Reviews, 102(2), 1025–1151.

57- Sennoga, C. A. (2020). Ultrasound imaging. In Elsevier eBooks (pp. 123–161).

58- Yang, T., Jin, Y., & Neogi, A. (2022). Acoustic attenuation and dispersion in fatty tissues and tissue phantoms influencing ultrasound biomedical imaging. ACS Omega, 8(1), 1319–1330.

59- Diagnostic Radiology: Advances in imaging technology. (n.d.). Google Books.

60- Bonosi, L., Marrone, S., Benigno, U. E., Buscemi, F., Musso, S., Porzio, M., Silven, M. P., Torregrossa, F., & Grasso, G. (2023). Maximal Safe resection in Glioblastoma surgery: A Systematic Review of advanced Intraoperative Image-Guided techniques. Brain Sciences, 13(2), 216.

61- Selbekk, T., Jakola, A. S., Solheim, O., Johansen, T. F., Lindseth, F., Reinertsen, I., & Unsgård, G. (2019). Ultrasound imaging in neurosurgery: approaches to minimize surgically induced image artefacts for improved resection control. *Acta Neurochirurgica*, *155*(6), 973–980.

62- Medical, L. (2023). Ultrasound transducer types and how to select the right transducer (2023). LBN Medical.

63- Geoghegan, R., Ter Haar, G., Nightingale, K. R., Marks, L. S., & Natarajan, S. (2022). Methods of monitoring thermal ablation of soft tissue tumors – A comprehensive review. Medical Physics, 49(2), 769–791.

64- Yonso, M., & Skalski, M. (2019). Acoustic shadowing. Radiopaedia.org.

65- Ryan's Retina E-Book. (n.d.). Google Books.

66-Atlas of Ultrasound-Guided Musculoskeletal Injections. (2021, December 7). Issuu.

67- Emergency and Clinical ultrasound Board review. (n.d.). Google Books.

68- Schmale, I. L., Vandelaar, L. J., Luong, A. U., Citardi, M. J., & Yao, W. C. (2020). Image-Guided Surgery and Intraoperative Imaging in Rhinology: clinical update and current state of the art. Ear, Nose, & Throat Journal, 100(10), NP475–NP486.